JOINT EUROPEAN TORUS

JET–P(92)73

L.R. Baylor, G.L. Schmidt, W.A. Houlberg, S.L. Milora, C. Gowers,
W. Bailey, M. Gadeberg, P. Kupschus, J.A. Tafle, D.K. Owens,
D.K. Mansfield, H. Park and JET Team

Pellet Fuelling Deposition Measurements on JET and TFTR

Pellet Fuelling Deposition Measurements on JET and TFTR

L.R. Baylor[1], G.L. Schmidt[2], W.A. Houlberg[1], S.L. Milora[1], C. Gowers, W. Bailey, M. Gadeberg, P. Kupschus, J.A. Tafle, D.K. Owens, D.K. Mansfield[2], H. Park[2] and JET Team*

JET-Joint Undertaking, Culham Science Centre, OX14 3DB, Abingdon, UK

[1]Oak Ridge National Laboratory, Oak Ridge, Tennessee, USA
[2]Princeton Plasma Physics Laboratory, Princeton, New Jersey, USA
** See Annex*

Preprint of Paper to be submitted for publication in
Nuclear Fusion

July 27, 1992

PELLET FUELING DEPOSITION MEASUREMENTS ON JET AND TFTR*

L.R. BAYLOR, G.L. SCHMIDT**, W.A. HOULBERG, S.L. MILORA,
C. GOWERS***, W. BAILEY***, M. GADEBERG***, P. KUPSCHUS***,
J.A. TAGLE***, D.K. OWENS**, D.K. MANSFIELD**, H. PARK**
Oak Ridge National Laboratory
Oak Ridge, Tennessee,
United States of America

ABSTRACT. The effective radial deposition profile of deuterium pellets injected into the Joint European Torus (JET) and Tokamak Fusion Test Reactor (TFTR) tokamaks has been determined from Thomson scattering diagnostic measurements of electron density taken immediately after pellet injection. The pellet ablation rate deduced from these measurements differs from that predicted by conventional pellet ablation theory. The possibility of enhanced radial transport during the ablation process has been examined to determine whether this can explain the difference between theory and experiment, but no evidence has been found to support such an explanation. The temporal evolution of the Balmer-alpha light emitted during pellet ablation is found to be different from the effective pellet ablation rate determined from the density profile measurements. We conclude that the shielding mechanisms of conventional pellet ablation models need modifications to predict and reproduce the observed effective ablation rate and penetration depth.

1. INTRODUCTION

Injection of frozen hydrogenic pellets for fueling magnetically confined plasmas has been studied in a number of laboratories for many years. Pellet fueling has the advantage over gas fueling of depositing the bulk of the fuel particles in the plasma core. Core fueling is an important issue for future tritium

*Research Sponsored by the Office of Fusion Energy, under Contract No. DE-AC05-84OR21400 with Martin Marietta Energy Systems, Inc.
**Princeton Plasma Physics Laboratory, Princeton, New Jersey, USA
***JET Joint Undertaking, Abingdon, Oxon, United Kingdom

experiments and may produce more peaked density profiles and higher fusion reaction rates than traditional edge fueling via gas puffing. Determining the deposition of the fuel particles from injected pellets is important in understanding the fueling profile that can be obtained from pellet injection and may yield a better understanding of the ablation process. Ablation theory has been investigated by many authors and has led to the neutral gas shielding (NGS) model reviewed in Ref. [1].

In this paper, we present measurements of electron density profiles taken immediately after pellet injection in both JET and TFTR. From these measurements we infer the effective pellet ablation rate needed to produce the resulting density profile. The measurements are made in both Ohmic and auxiliary heated discharges. We then compare these results to the measured light emission from the ablating pellets and to the ablation rate predicted by conventional models of pellet ablation.

In the following sections we first discuss the measurements of electron density profiles and light emission from ablating pellets. We then present a description of the effective ablation rates calculated from the density profile data, a comparison with pellet ablation theory, and finally a discussion of the results.

2. EXPERIMENTAL MEASUREMENTS

The determination of pellet deposition uses measurements of pellet speed and mass, plasma density profiles before and immediately following the pellet, pellet penetration, and loss of mass during injection.

2.1. Measurements of pellet parameters

The pellet injectors used on JET and TFTR for this investigation were both developed at Oak Ridge National Laboratory and use single-stage light gas guns to accelerate deuterium pellets to speeds approaching 1400 m/s [2,3]. The pellets are nominally cylinders of equal length and diameter.

The pellet injection systems on both JET and TFTR inject the pellets on or near the horizontal midplane of the device. The JET injection system uses microwave cavities located along the injection line to measure the pellet mass

and the pellet speed. The speed is determined with an accuracy of $\pm 0.3\%$, which yields a ± 0.05 m uncertainty in the penetration depth from the time-of-flight measurement assuming constant radial speed [4]. The TFTR injection system [3] uses light gates in the injection line to determine the pellet speed, giving an accuracy within $\pm 0.5\%$. This translates to a ± 0.04 m uncertainty in the penetration depth.

2.2. Density profile measurements

Measurements of the density profiles before and after deuterium pellet injection are used to determine the effective pellet source. The JET and TFTR tokamaks both have Thomson scattering diagnostics which provide accurate electron density profiles with good spatial resolution suitable for this measurement. The JET LIDAR (**LI**ght **D**etection **A**nd **R**anging) Thomson scattering diagnostic uses a ruby laser that is directed radially in the equatorial plane and collects the 180° backscattered light [5]. The measurements have a spatial resolution of 0.10 m, limited by the finite pulse length of the laser light. The LIDAR measurement is made 120° toroidally from the pellet injection line. The TFTR Thomson scattering diagnostic is located 48° toroidally from the pellet injection line and also uses a ruby laser directed radially but collects scattered light at 90° [6]. The scattered light is focused onto 76 optical fibers and detected by a charge coupled device, yielding a radial resolution of 0.024 m. In addition, far-infrared interferometers (6 channel on JET and 10 channel on TFTR) are used to determine the pre-pellet density profile.

An example of Thomson scattering measurements from JET is shown in Fig. 1(a), which shows the density profile 2.5 ms after injection of a 2.7 mm pellet and the density profile from an identical 3 MA discharge with 9 MW neutral beam injection (NBI). The pellet penetration depth, determined from soft X-ray data, is shown as a vertical dashed line and agrees with the measured density increase. The difference between the two density profiles represents the effective pellet deposition. There is some difference in density on axis which is due to sawtooth activity and not to the injected pellet.

A density profile determined from Thomson scattering data taken 18 ms after injection of a 3.0 mm pellet into an Ohmic TFTR discharge is shown in Fig.

2(a). This pellet represents a 200% perturbation to the plasma density. The density profile obtained from inversion of the 10 channel far-infrared interferometer data, before the pellet is injected, is also shown. The pellet penetration depth shown in this figure is determined from the broadband light emission and is in general agreement with the region of largest density increase. The increase in density in the plasma core has most likely arisen from a sawtooth relaxation triggered by the injected pellet (inversion radius of 8 cm determined from soft X-ray data) and subsequent diffusion. The electron temperature profiles before and after pellet injection are shown in Fig. 2(b).

2.3. Balmer-alpha emission

In both JET and TFTR, the light emitted by the pellets injected into the plasma has been used as a monitor of the pellet ablation rate. As ionization takes place in the ablatant, the excited states of the deuterium atoms are also populated. Transitions between excited states result in line emission. One such transition is the Balmer-alpha ($n = 3 \rightarrow 2$) transition, which is referred to as D_α line emission (centered at 6561.0 $\AA$).

On JET, the D_α line and broadband light emission were measured by photodiodes through a wide-angle periscope system [7]. By comparing the signals from two photodiodes, one using a 100 $\AA$ wide filter centered on the D_α line and the other with no filter (broadband), we have been able to confirm that the broadband light emission from pellet ablation on JET is strongly dominated by the D_α light. More than 75% of the emission intensity measured by the broadband detector was associated with the D_α line. On TFTR, the broadband emission is measured by a photodiode viewing from the injection line behind the pellet entry point. Photographic data of the ablation light emission were not available from either device for the experiments reported in this paper.

2.4. Additional measurements

A vertical soft X-ray camera is located on JET above the torus where the pellet enters the plasma, and its data can be used to determine the pellet penetration and trajectory. The penetration depth of the pellet from the soft X-ray

data agrees well with the penetration determined from the duration of the D_α emission [4,8]. The soft X-ray data from the vertical camera and from horizontal cameras seem to indicate a straight trajectory through the plasma for the pellets in the discharges studied. The toroidal extent of the soft X-ray data is ± 30 cm, and the pellet does not leave the observation window. Hard X-ray detectors on JET give no indication that a strong non-thermal electron population exists in any of the JET discharges studied.

Langmuir probes are located at different positions around the torus in JET to measure the particle flux in the scrape-off region. Two probes are located at the horizontal midplane on ICRF antenna limiters and are displaced 30° and 150° toroidally from the pellet entry point. An array of probes is also located in the upper x-point region. A fast response ion gauge is located on TFTR just above the pellet entry point on the horizontal midplane. Both the probes and ion gauge are used to measure the quantity of pellet mass that may be lost in the scrape-off region during injection of the pellet.

3. EFFECTIVE ABLATION RATE

The question arises whether the density profile measurement after injection is a good indication of the pellet ablation rate. Three time scales must be considered to answer this question. The time scale of the pellet entering the plasma and ablating, τ_{abl}, is very short, on the order of 700 μs. The transport time of the ablatant along the field lines, $\tau_{\|}$, is also very short; the measured velocity of the density perturbation on TFTR is 1.5×10^5m/s [9], yielding transport times on the order of a few hundred microseconds. The diffusive time scale for the density, τ_{diff}, is much longer, as the particle diffusivity in the density decay of pellet fueled plasmas is generally less than 1.0 m^2/s [8], which suggests only a modest diffusion of the density in the time between injection and density profile measurement. It is possible, though, that the local perturbation of the pellet may excite additional transport on a shorter time scale than τ_{diff}.

Electron pressure profiles calculated from the Thomson scattering data have been examined to look for a non-adiabatic response to the ablating pellet. An example of pressure profiles for two identical discharges (one with and

one without an injected pellet) are shown in Fig. 1(b); within the error bars of the measurements, they are the same over the region of pellet deposition. This indicates that the processes which result in the effective pellet deposition are locally adiabatic within the experimental uncertainty.

Measurements from the vertical soft X-ray camera and fast electron cyclotron emission (ECE) diagnostic on JET with a time resolution of 5 μs have been examined and show no indication of a fast plasma perturbation across the entire plasma minor radius in the few milliseconds between pellet injection and the Thomson scattering density measurement in the discharges studied. If the ablatant before ionization were moving radially within the plasma, one would expect to see a perturbation in the soft X-ray data, since the bulk of the X-ray power would be coming from bremsstrahlung radiation caused by collisions between the ablated particles and the incident electrons. In some cases not included in these studies, MHD effects triggered by the injected pellet appear as strong perturbations in the soft X-ray data.

The line-integrated density through the center of the plasma typically changes much less than 1% in the short time interval between injection and the density profile measurement in the data presented; therefore, because of the adiabatic response of the plasma and the lack of evidence of any strong perturbations, we believe that the measured profiles reflect the deposition by the pellet.

We define the effective ablation rate for pellets injected into JET and TFTR as the ablation rate needed to reproduce the measured density profile immediately after injection and then compare this rate with theoretical ablation rates. The effective ablation rate is calculated from the effective deposition profile by using the relation

$$\dot{N}_{\mathrm{eff}} = \Delta n_{ei}\, \Delta V_i\, v_p/\Delta r_i \qquad (1)$$

where Δn_{ei} is the deposition density at the ith radial grid location, ΔV_i is the volume between the ith and $(i+1)$th radial grid locations, Δr_i is the radial grid spacing, and v_p is the pellet velocity. It is assumed that the pellet trajectory in the plasma is straight, the pellet speed is constant, and the ablated pellet material is ionized near the pellet surface and confined on the flux sur-

face where it is ionized. The symmetric density profiles measured after pellet injection (examples shown in Figs. 2 and 3) are verification that the ablated pellet material is confined on and uniformly distributed over the flux surfaces.

Electron density profiles from three JET discharges measured after injection of 4 mm pellets in Ohmic plasmas are shown in Fig. 3(a) as a function of major radius. These profile measurements were made with the JET LIDAR Thomson scattering diagnostic 4 ms after pellet injection. The pre-pellet density profile (dotted line) is obtained by inversion of data from a 6 chord far-infrared interferometer. This density profile is subtracted from the post-pellet density profiles to obtain the effective pellet deposition profiles in Fig. 3(b). The electron temperature profiles before injection (from ECE) and after injection (from LIDAR) are shown in Fig. 3(c). The calculated effective ablation rates for the pellets in Fig. 3 are shown in Fig. 4 as a function of radius. All three cases show that the effective ablation rate is strong near the plasma edge and decreases as the pellet approaches the plasma center. The three injected pellets were measured to have virtually identical mass and were injected into identical discharges. It appears that the differences in the effective ablation rates of the three cases in Fig. 4 are due primarily to some random process.

It is possible from the measured effective particle deposition profiles to integrate the total number of particles deposited by the pellet, $\int n_d dV$. By comparing the number of particles deposited with the measured pellet mass, we can determine the pellet mass deposition efficiency. From the deposition data shown in Fig. 3, we calculate a total particle deposition of $(3.6 \pm 0.1) \times 10^{21}$ for the three cases, which agrees well with the measured mass for these 4.0 mm pellets (100% fueling efficiency).

LIDAR electron density profiles before and after injection of a 4 mm pellet into a JET H-mode discharge are shown in Fig. 5. LIDAR can be used for the preinjection density profile since the discharge density is constant during the period before the pellet is injected, as measured by the interferometer. The effective deposition profile is also plotted. In cases where pellets are injected into auxiliary heated plasmas, the fueling efficiency has been shown to decrease substantially [8,10]. For this pellet, injected into an H-mode discharge, the deposition measurement gives a total particle deposition of 1.6×10^{21}, which is

only $\sim$ 50% of the measured pellet mass. The calculated effective ablation rate for this pellet is shown in Fig. 6. It is similar to the Ohmic cases in Fig. 4 in that the effective ablation rate is strong at the plasma edge (even stronger in this case) and decreases as the pellet penetrates deeper into the plasma. The D_α emission from the ablating pellet is plotted on the same radial scale after being converted from its time base to major radius. We see that the effective ablation rate is quite different from the measured D_α emission.

The calculated effective ablation rate and the broadband emission from the ablating pellet are shown in Fig. 7 for the pellet injected into the TFTR Ohmic discharge in Fig. 2. The broadband emission rate and the effective ablation rate is similar to that in Fig. 6 for the JET case. The D_α emission from the pellets in both devices is much stronger toward the end of the pellet trajectory where the effective ablation rate is much reduced from its value nearer the plasma edge. The D_α emissions from both devices also demonstrate similar levels of fluctuations.

4. COMPARISON WITH THEORY

Most theoretical predictions of pellet ablation have used the classical NGS model [1,11]. The NGS model is based on a spherically symmetric neutral ablation cloud and neglects the effects of the magnetic field. The source of neutral gas in the cloud is determined by the heat flux at the pellet surface, which is attenuated by the ablated neutral gas (self-shielding). A simplified relationship between the pellet ablation rate $\dot{N}_p$, the effective spherical pellet radius r_p, and the background plasma electron density n_e and temperature T_e is given approximately by [4]

$$\dot{N}_p \propto {n_e}^{1/3} {T_e}^{5/3} {r_p}^{4/3} \tag{2}$$

Pellet ablation calculations using the NGS model in the PELLET code of Houlberg et al. [12] have been made for the cases reported here using an equivalent spherical pellet radius and a minimum neutral cloud radius of 1 mm. A Maxwellian distribution is used for the incident electrons in the calculation.

Significant additional shielding (amplification of the neutral gas stopping cross-section), which is not varied with plasma parameters, is required to bring the NGS model into agreement with the experimental penetration depth [4]. We identify this NGS model with enhanced shielding as NGS+.

Figure 4 shows a comparison of the NGS+ model calculation results with the effective ablation rate for the 4 mm pellets injected into JET as shown in Fig. 3. The model calculations use the measured electron temperature and density profiles at a time just before the pellet is injected. The NGS+ model shows much lower ablation at the plasma edge and higher ablation towards the end of the pellet trajectory than the effective ablation rates from the density profile measurements. The NGS model with a monoenergetic electron distribution yields an ablation rate profile for this case that is virtually the same as the NGS+ model.

The effective ablation rate for the 4 mm pellet injected into a JET H-mode discharge shown in Figs. 5 and 6, is compared in Fig. 8 with the results of calculations using the NGS model, with and without enhanced shielding, and the neutral gas plus plasma shielding (NGPS) [12] model. The agreement is not particularly good with any of the models. The profile of the NGS+ model ablation rate is typically much closer to the profile of the D_α emission rate (shown in Fig. 6) than to the effective ablation rate. Also shown in Fig. 8 is the ablation rate that would exist if the total plasma electron energy flux incident on the pellet and cloud were converted to pellet sublimation, given by

$$\dot{N}_i = Q_e A_p / \lambda_s \ , \tag{3}$$

where Q_e is the incident electron energy flux, A_p is the effective pellet area, and λ_s is the molecular heat of sublimation (1.5×10^{-2} eV for D_2). The effective pellet area is calculated using the equivalent pellet radius inferred from the integral of $\dot{N}_{eff}$, which is independent of any pellet mass lost from the plasma during the ablation process. The incident electron energy flux is given by

$$Q_e = \frac{4}{3}\left(\frac{n_e \bar{v}_e}{4} E_e\right) = \frac{n_e k T_e}{2}\left(\frac{8kT_e}{\pi m_e}\right)^{1/2} \tag{4}$$

where n_e and T_e are the electron density and temperature. If we take the ratio $\dot{N}_i/\dot{N}_{eff}$, we have a factor that represents the magnitude of attenuation that the incident electron energy flux undergoes from the pellet shielding mechanisms. We plot this attenuation factor in Fig. 9 for the pellet of Fig. 8 and note that it increases dramatically with penetration depth. Also plotted in Fig. 9 are the attenuation factors for the NGS model and the NGS+ model, both with Maxwellian electron distributions. The models predict significantly more attenuation of the incident heat flux near the plasma edge than is inferred from the data.

The D_α emission rate has been assumed to be proportional to the ablation rate of the pellet by a number of authors [1,13] under the assumption of a collisional-radiative model with cloud electron temperature greater than 20 eV. A comparison of the time-dependent effective ablation rate, as determined from the density profile measurements, with the measured D_α emission from both JET and TFTR has shown that the photon yield and the effective ablation rate do not seem to be well correlated. In simulations of pellet ablation using a flux limiting thermal conduction model, Dunning et al. [14] calculated the D_α emission with a population level equilibrium model in which collisional excitation is balanced by collisional and radiative de-excitation. They came to the conclusion that the ablation rate and the D_α emission rate were not proportional. McNeill et al. [15] measured the electron temperature of the pellet cloud in TFTR to be on the order of 1.5 eV, which is low enough to call into question the assumption that the D_α emission rate is proportional to the ablation rate.

5. DISCUSSION

Ideally, the radial profile of the pellet ablation rate, $\dot{N}_p$, and the effective pellet particle deposition profile, $\Delta n_e\, dV$, should coincide since the pellet speed remains constant along the pellet trajectory and fuel particles are distributed rapidly over the flux surface where they are released. Our effective ablation rate calculations have assumed this ideal condition; however, it is possible

that other processes may exist that mask the true ablation rate by causing the plasma density profile to readjust on a very fast time scale.

One possible explanation for the apparent strong deposition near the outer edge of the plasma would be a fast perturbation ($<$ 1 ms) in the plasma that quickly moves mass from the pellet ablatant in the plasma core toward the edge. However, as stated earlier, measurements of soft X-rays and plasma electron temperature with high time resolution show no indication of significant mass moving radially in the plasma immediately after or during the pellet ablation process. The constancy of the plasma pressure profile through the pellet injection event, as discussed earlier (Fig. 1(b)), indicates that little plasma energy is involved in any radial mass movement. This would imply that radial movement of the pellet ablatant is taking place before the ablatant is thermalized.

It has been suggested that strong diffusive effects, occurring on a microsecond time scale while the pellet is ablating in the plasma, cause a strong radial smoothing of the density profile during injection. If this were the case, one would expect inward as well as outward diffusion since the local density gradients near the pellet are strong in both directions. However, the measured density profiles always show strong deposition displaced radially outward when compared to the NGS model, which makes it unlikely that density gradient-driven diffusive effects alone are masking the deposition profile from the NGS model. It is possible, though, that fast particle transport effects driven by cross-terms of the transport equations could be important locally and affect the resulting deposition profile.

Data from both JET and TFTR have shown a strong discrepancy between the effective ablation rate and the NGS model. Results from other experiments, notably ASDEX [16], have implied that the ablation rate in the outer plasma region is higher than expected from the NGS model. Pellet penetration experiments on JET [4] have verified that the NGS model without additional shielding consistently predicts lower pellet penetration depths than those measured. The addition of a plasma shield to the model improves the agreement at a fixed velocity but fails to reproduce the scaling of penetration with pellet velocity. Additional modeling of pellet penetration data from several tokamaks

[17] also showed that none of the variations of the NGS model could consistently predict the measured pellet penetrations. It is therefore apparent from the effective ablation rate results here and from pellet penetration studies that additional shielding effects, such as ellipticity of the neutral shield, magnetic shielding, and electrostatic potential, must be taken into account to fully explain the observed local ablation of hydrogenic pellets in fusion-grade plasmas. However, none of the additional shielding effects mentioned would act to increase the edge ablation to levels that are implied by the data presented here.

Some previous pellet injection experiments, including those on Alcator-C [18] and TFR [19], have revealed a cold wave propagating in front of the pellet that presumably affected the ablation rate as the pellet moved inward. There is no indication in either the JET or the TFTR fast ECE data of a cold wave traveling radially inward faster than the pellet. In JET however, when the pellet crosses the $q = 1$ surface, a sharp reduction in temperature is triggered within the $q = 1$ surface [8,20]. This is similar to results reported from JIPP T-IIU [21]. In the cases on JET where the pellet crosses the $q = 1$ surface, the resulting density profile is quite hollow, indicating that the rapid cooling within the $q = 1$ surface may be reducing the ablation rate within that surface.

Another issue with our understanding of pellet ablation is the mass that is lost when pellets are injected into plasmas with substantial auxiliary heating. It has been found in more than one tokamak experiment that a substantial fraction of the pellet mass is missing from the plasma after injection into auxiliary heated plasmas [8,10,22,23]. In experiments on JET, single 4 mm pellets were injected into both Ohmic heated and H-mode NBI + ICRH discharges. Examples of the resulting density profiles from these experiments are shown in Fig. 3 and 5. The particle flux in the scrape-off region was measured with the Langmuir probes discussed in Section 2.4. We find substantial particle flux to the probes in the X-point region of the discharge and significant flux to midplane mounted probes when pellets are injected into auxiliary heated plasmas. The midplane probe located closer to the pellet entry point (30° toroidally displaced versus 150°) shows almost 10 times the particle flux of the other midplane probe, and the flux reaches that probe 0.5 ms sooner. Figure 10(a) shows the relative magnitude and timing of the probe saturation currents in an H-

mode plasma. When pellets are injected into Ohmic plasmas with the same magnetic configuration, the probes show no increase in the saturation current when the pellet enters the plasma, as shown in Fig. 10(b).

The amount of mass missing from the deposition measurements correlates well with the increased particle flux seen by the probes in the scrape-off region. Edge measurement of neutral pressure in Tore Supra has shown a sharp rise in neutral pressure following pellet injection into discharges with lower hybrid current drive [23] but no such rise in Ohmic discharges. The pressure rise correlates with lost pellet mass, which presumably results from enhanced peripheral pellet ablation from a known suprathermal electron population. Data from an ion gauge located near the pellet entry point on TFTR have also shown a neutral pressure burst when pellets are injected into NBI heated plasmas as shown in Fig. 11. Ohmic discharges do not show the pressure burst when a pellet is injected except when the plasma is configured with a large minor radius running near the outside wall.

The mass loss that occurs during injection into auxiliary heated plasmas is not likely to come from enhanced ablation in the scrape-off plasma from fast ions because the fast ion density there is not thought to be large enough to cause appreciable ablation. The presence of suprathermal electrons does not seem likely (except in the Tore Supra case mentioned above), nor is there evidence of an extremely fast temperature relaxation, which connects inner and outer regions via parallel transport, as proposed by Büchl et al. for ASDEX [16].

6. SUMMARY

The effective deposition from injected deuterium pellets in JET and TFTR has been measured and used to calculate the effective ablation rate of the pellets. The effective ablation rate differs from that predicted by the conventional NGS model. In both devices, the effective ablation rate is higher in the outer region of the plasma and lower in the core region than predicted by the theory. The penetration depth of the pellets, however, scales similarly to the predictions of the NGS model [4], in particular the pellet velocity scaling. However,

the NGS model with a Maxwellian electron distribution required significant additional shielding for modeled pellets to reach the measured penetration depth. It is clear that shielding mechanisms in addition to the neutral gas shield, such as magnetic shielding and electrostatic potential, are needed to explain the observed penetration depth and effective ablation rate. Questions that remain about fast particle and heat transport during pellet injection and about lost pellet mass during auxiliary heating may be resolved by future measurements. Nonetheless, the resulting effective deposition profile from pellet injection is most important because it is what determines the effective fueling source.

Measurements of broadband light emission and D_α emission from ablating pellets have been compared to the effective ablation rate determined from the effective deposition. The broadband emission primarily consists of D_α emission and is a poor indication of the effective ablation rate. The D_α emission rate seems to be more closely related to the magnitude of the heat flux incident on the pellet than to the effective ablation rate.

Understanding the discrepancy between pellet ablation theory and experiment that has been presented here is important for better understanding of the ablation from hydrogenic pellets. This discrepancy makes a significant difference in the resulting density profile obtained from non-central penetration of pellets. Because this is the expected case for future devices such as ITER, we need to better understand both the ablation and shielding physics and the plasma response to pellet injection in order to predict the effect that pellet injection may have on fueling and confinement in an ignition device.

ACKNOWLEDGEMENTS

The authors gratefully acknowledge the contributions of the JET and TFTR experimental and operational teams. Part of this work was performed under a collaboration agreement between the JET Joint Undertaking and the U.S. Department of Energy.

REFERENCES

[1] MILORA, S.L., J. Fusion Energy **1** (1981) 15.

[2] MILORA, S.L., COMBS, S.K., BAYLOR, L.R., et al., in Proc. 12th IEEE Symposium on Fusion Engineering (Monterey, 1987), Vol. 2, IEEE, New York (1987) 784.

[3] COMBS, S.K., MILORA, S.L., FOUST, C.R., et al., Rev. Sci. Instrum. **58** (1987) 1195.

[4] HOULBERG, W.A., BAYLOR, L.R., MILORA, S.L., et al., Pellet Penetration Experiments on JET, submitted to Nucl. Fusion.

[5] SALZMANN, H., HIRSCH, K., NIELSEN, P., et al., Nucl. Fusion **27** (1987) 1925.

[6] JOHNSON, D., BRETZ, N., DIMOCK, D., et al., Rev. Sci. Instrum. **57** (1986) 1856.

[7] BAILEY, W., KUPSCHUS, P., GADEBERG, M., et al., in Fusion Technology (Proc. 15th Symp. Utrecht, 1988), Vol. 1, North Holland, Amsterdam (1989) 720.

[8] BAYLOR, L.R., Particle Transport in Pellet-Fueled JET Plasmas, PhD Thesis, Univ. of Tennessee, Knoxville (1989).

[9] MANSFIELD, D.K., JANOS, A., OWENS, D.K., et al., Phys. Rev. Lett. **66** (1991) 3140.

[10] OWENS, D.K., SCHMIDT, G.L., CAVALLO, A., et al., in Pellet Injection and Toroidal Confinement (Proc. Tech. Committee Meeting, Gut Ising, 1988), IAEA-TECDOC-534, IAEA, Vienna (1989) 191.

[11] PARKS, P.B., TURNBULL, R.J., FOSTER, C.A., Nucl. Fusion **17** (1977) 539.

[12] HOULBERG, W.A., MILORA, S.L., ATTENBERGER, S.E., Nucl. Fusion **28** (1988) 595.

[13] CHANG, C.T., THOMSEN, L., Nucl. Fusion **24** (1984) 697.

[14] DUNNING, M.J., MAYER, F.J., KAMMASH, T., Nucl. Fusion **30** (1990) 919.

[15] McNEILL, D.H., GREENE, G.J., NEWBURGER, J.D., OWENS, D.K., Phys. Fluids B **3** (1991) 1994.

[16] BÜCHL, K., VLASES, G.C., SANDMANN, W., LANG, R., Nucl. Fusion **27** (1987) 1939.

[17] GOUGE, M.J., HOULBERG, W.A., MILORA, S.L., Fusion Technol. **19** (1991) 95.

[18] GREENWALD, M., GWINN, D., MILORA, S.L., Phys. Rev. Lett. **53** (1984) 352.

[19] TFR Group, Nucl. Fusion **27** (1987) 1975.

[20] CHEETHAM, A.D., CAMPBELL, D.J., GONDHALEKAR, A., et al., in Controlled Fusion and Plasma Physics (Proc. 14th Eur. Conf. Madrid, 1987), Vol. 11D, Part I, European Physical Society, (1987) 205.

[21] SAKAMOTO, M., SATO, N., OGAWA, Y. et al., Plasma Phys. Controlled Fusion **33** (1991) 583.

[22] DRAWIN, H.W., GERAUD, A., Nucl. Fusion **29** (1989) 1681.

[23] CHATELIER, M., CEN, Cadarache, personal communication, 1992.

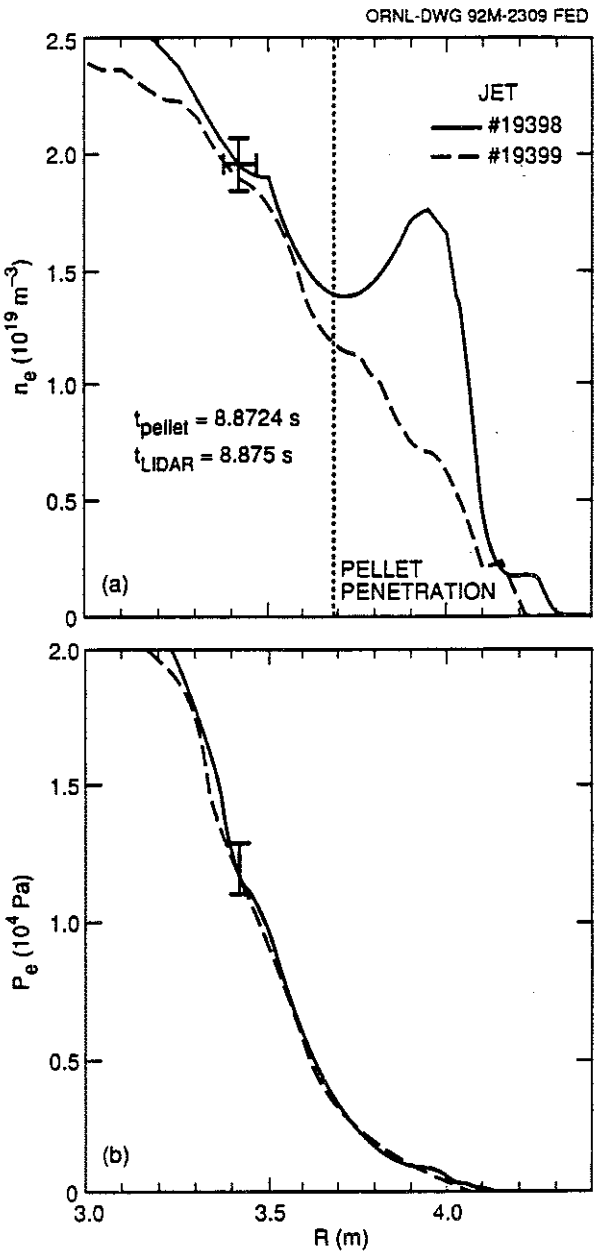

FIG. 1. Profiles of (a) electron density and (b) electron pressure, measured by LIDAR Thomson scattering, in a JET discharge 2.5 ms after a 2.7 mm deuterium pellet is injected and from an identical discharge with no pellet.

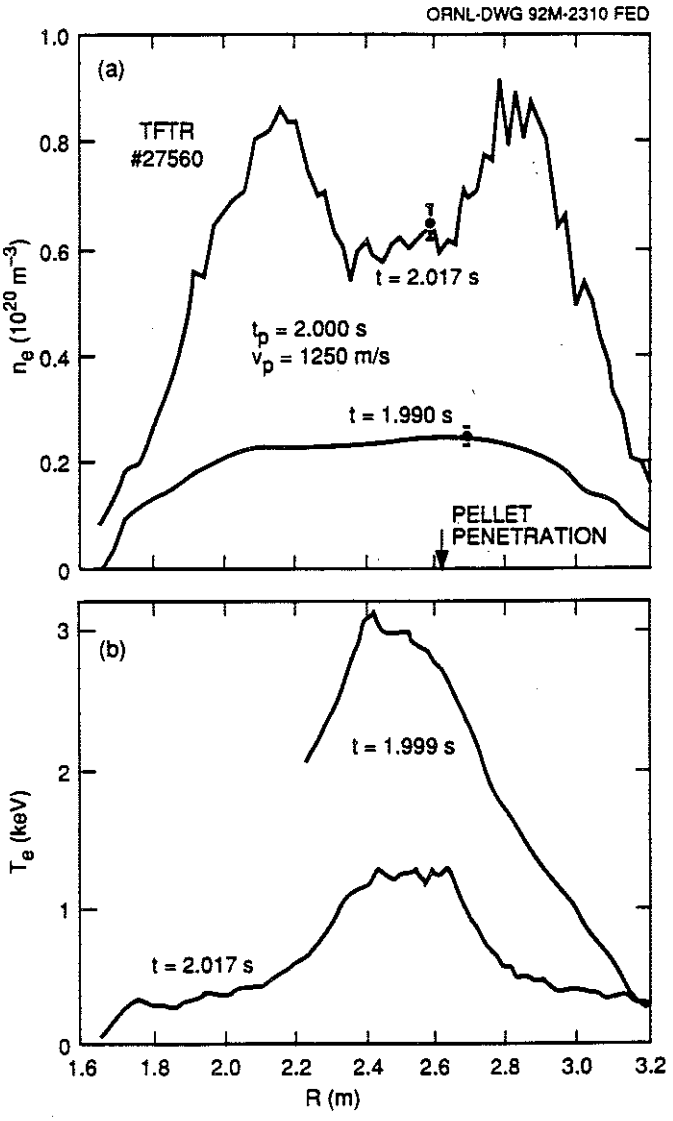

FIG. 2. (a) Electron density profile, from Thomson scattering data taken 18 ms after a 3.0 mm deuterium pellet is injected into an Ohmic TFTR discharge. The pre-pellet density profile (labelled t = 1.990 s), obtained from the inversion of far-infrared interferometer data is also shown. The pellet penetration depth determined from the broadband emission data is 2.62 m. (b) Electron temperature profile before injection (t = 1.99 s), measured by ECE, and after injection, from Thomson scattering data.

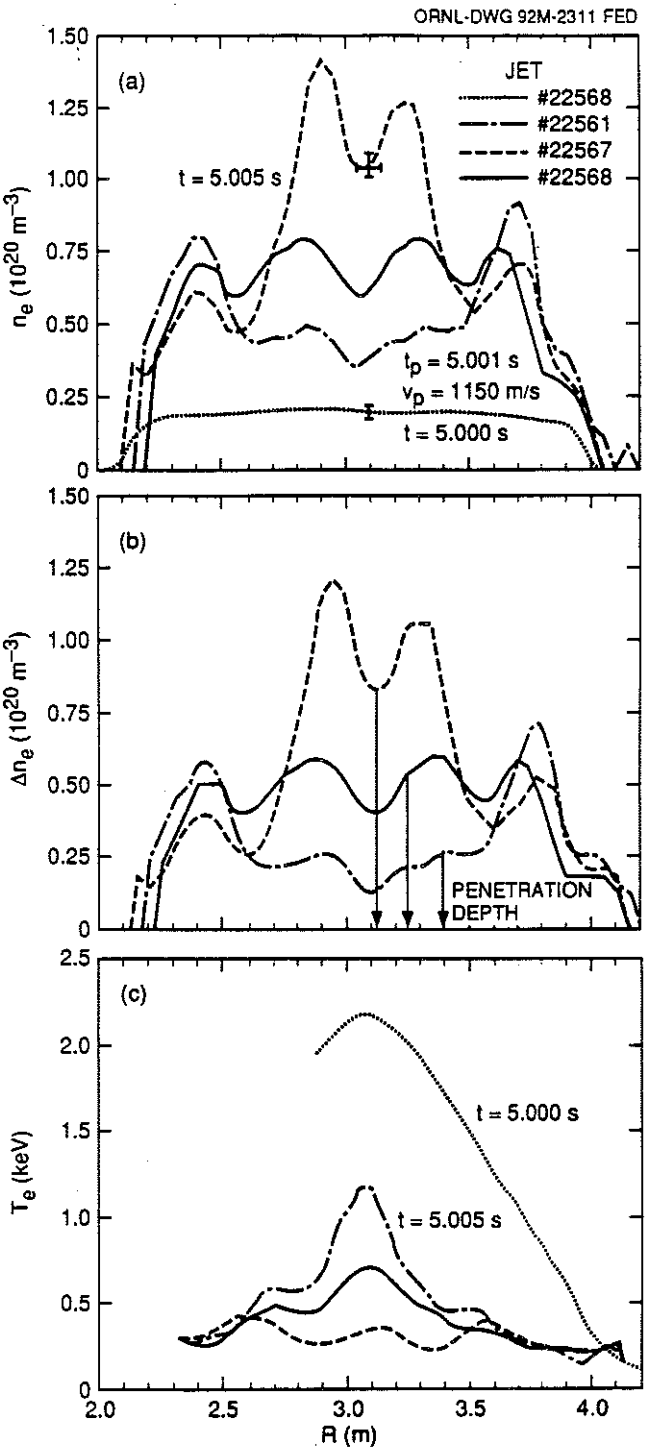

FIG. 3. (a) Electron density profiles from three JET Ohmic discharges measured by LIDAR Thomson scattering 4 ms after 4 mm deuterium pellet injection. The density profile before pellet injection, determined from inversion of interferometer data, is also shown. (b) Effective deposition profiles for these three JET discharges. The pellet penetration depth from D_α measurements is displayed for each of the three cases. (c) Electron temperature profiles after injection, measured by LIDAR Thomson scattering, and a typical temperature profile before injection, measured by ECE.

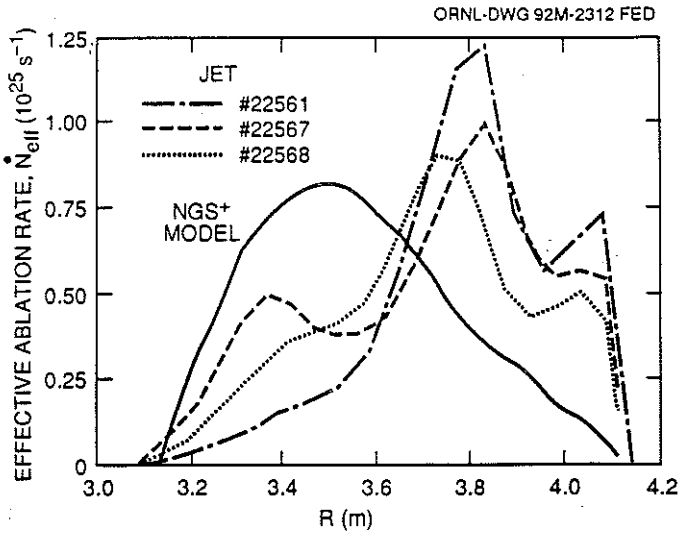

FIG. 4. Effective ablation rates calculated for the pellets of Fig. 3 mapped onto the radial location of the pellet trajectory. The solid line shows the ablation rate calculated from the NGS model with enhanced shielding (NGS+) for one of the discharges.

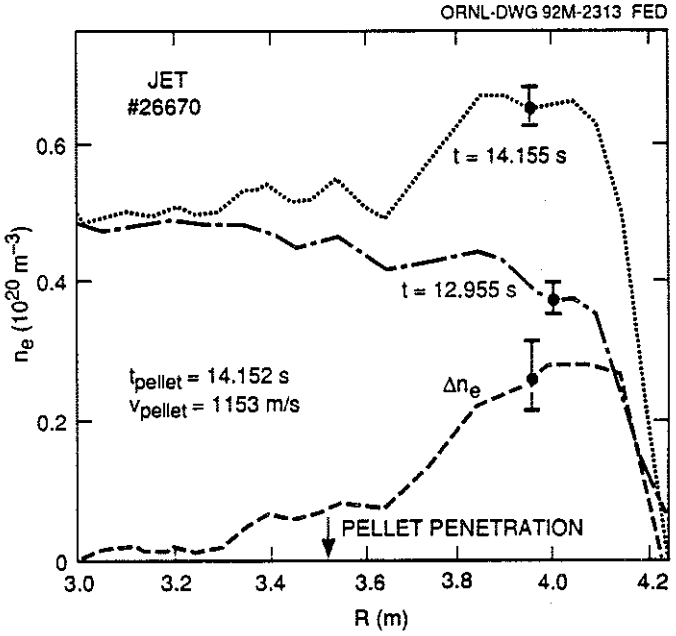

FIG. 5. The density profiles before and 3 ms after a 4 mm deuterium pellet is injected into a steady-state JET H-mode plasma (9 MW NBI, central $T_e = 3.1$ keV). The dashed line, labeled Δn_e, is the difference in the two profiles showing the effective pellet deposition. The pellet penetration depth determined from soft X-ray measurements is 3.52 m.

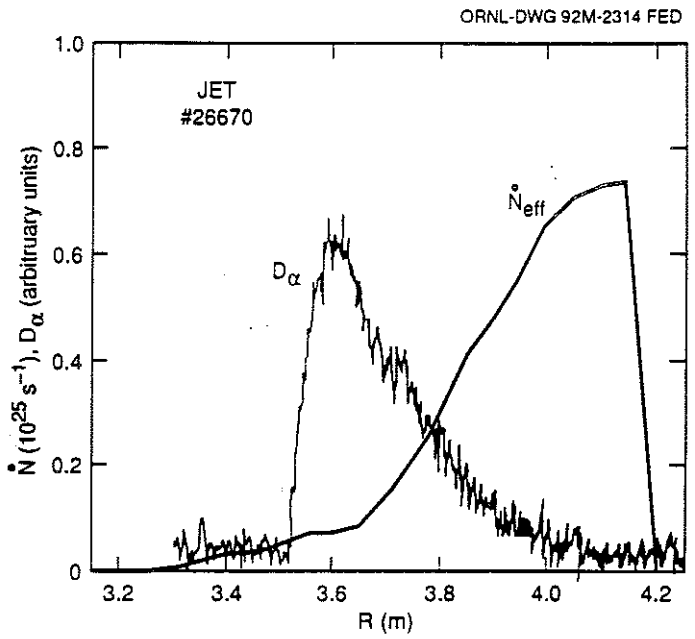

FIG. 6. The effective ablation rate profile for the 4 mm deuterium pellet of Fig. 5 and the D_α emission from the ablating pellet as functions of major radius.

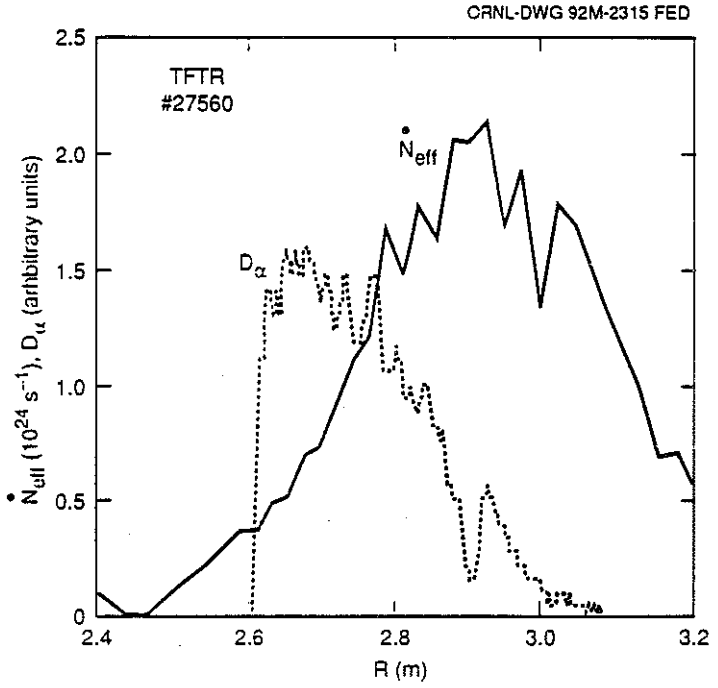

FIG. 7. The effective ablation rate profile for the 3.0 mm deuterium pellet of Fig. 2 and the broadband light emission from the pellet as functions of major radius.

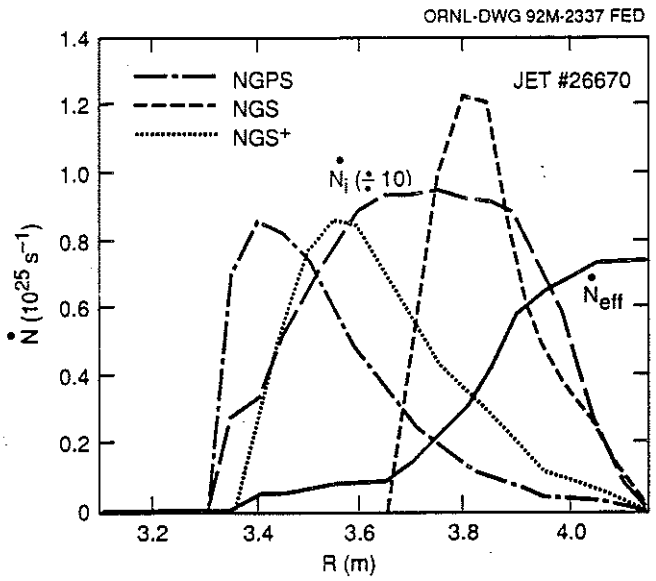

FIG. 8. The effective ablation rate for the pellet of Fig. 5 and ablation rates from the PELLET code [12], calculated using the neutral gas shielding (NGS), neutral gas shielding with enhanced shielding (NGS+), and neutral gas and plasma shielding (NGPS) models. The incident heat flux equivalent ablation rate $\dot{N}_i$ is also shown scaled down by a factor of 10.

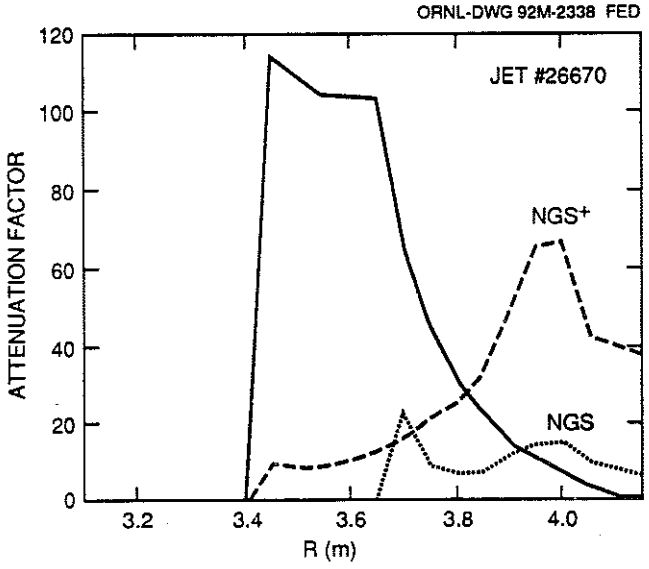

FIG. 9. The shielding attenuation factor, $(\dot{N}_i/\dot{N}_{eff})$, for the pellet of Fig. 5 as a function of plasma major radius. The attenuation factors for the NGS model and NGS+ model with enhanced shielding are also shown.

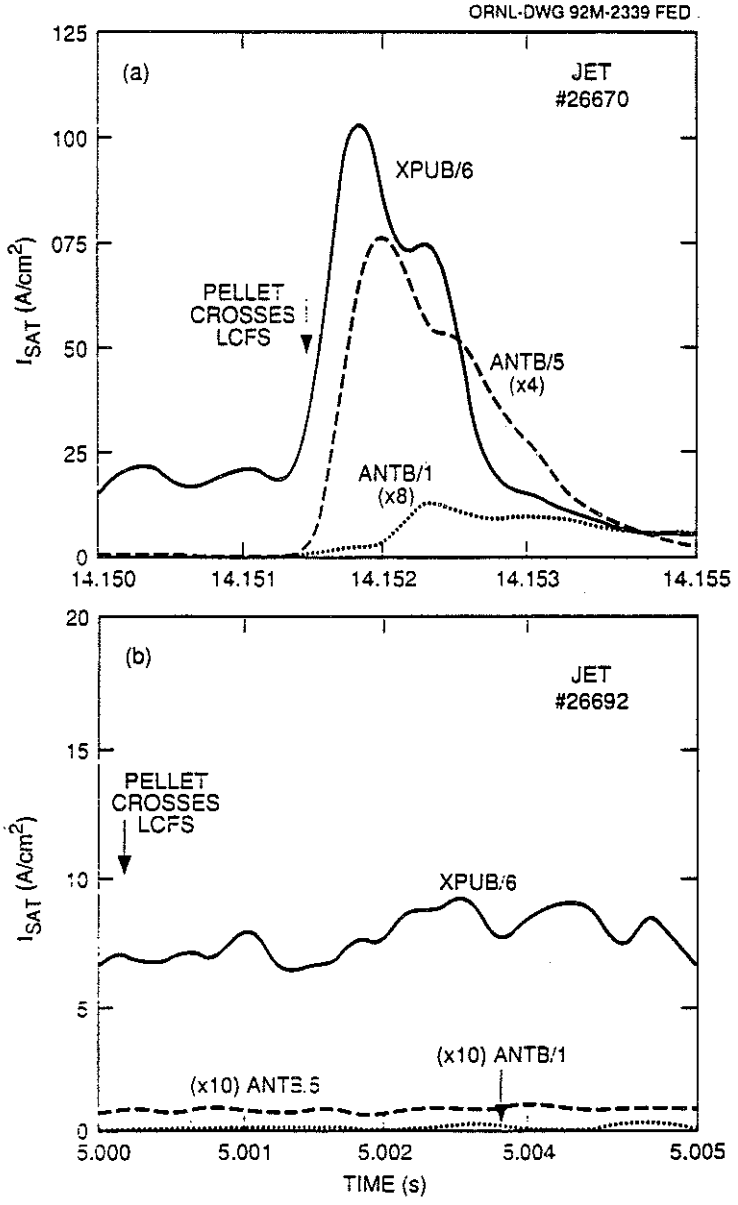

FIG. 10. The electron saturation current measured on midplane antenna probes (ANTB/5 and ANTB/1) and on an X-point probe (XPUB/6) in JET (a) with 4 mm pellet injection into an H-mode discharge and (b) with a 4 mm pellet injected into an Ohmic discharge.

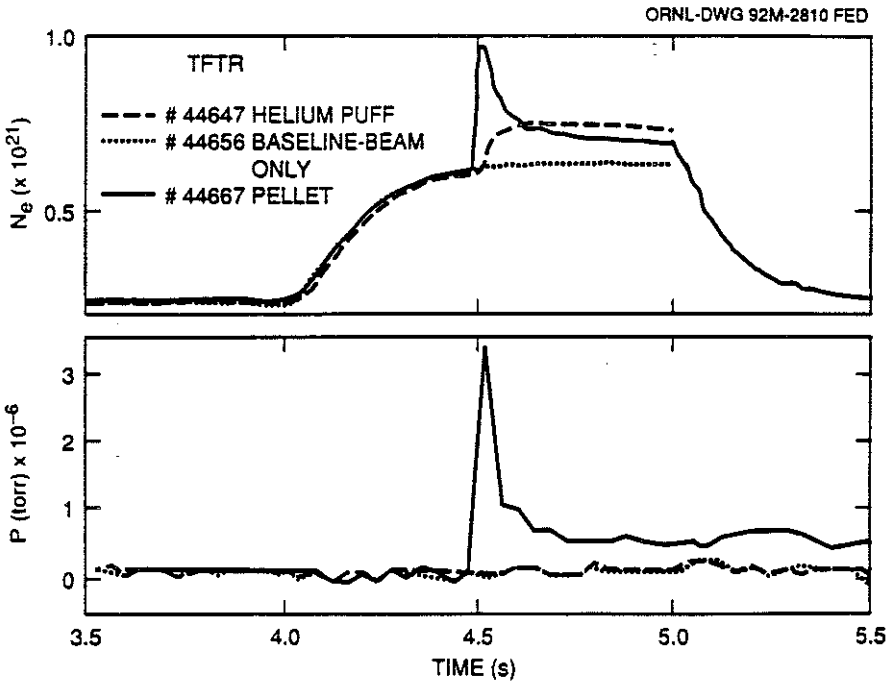

FIG. 11.(a) The total number of electrons in three TFTR discharges with NBI. A 4 mm pellet is injected at 4.5 s in #44667. (b) The neutral pressure measured by an ion gauge near the pellet entry point for the three discharges, showing an sharp increase only for the pellet fueled case.

Appendix I

THE JET TEAM

JET Joint Undertaking, Abingdon, Oxon, OX14 3EA, U.K.

J.M. Adams[1], B. Alper, H. Altmann, A. Andersen[14], P. Andrew, S.Ali-Arshad, W. Bailey, B. Balet, P. Barabaschi, Y. Baranov, P. Barker, R. Barnsley[2], M. Baronian, D.V. Bartlett, A.C. Bell, G. Benali, P. Bertoldi, E. Bertolini, V. Bhatnagar, A.J. Bickley, D. Bond, T. Bonicelli, S.J. Booth, G. Bosia, M. Botman, D. Boucher, P. Boucquey, M. Brandon, P. Breger, H. Brelen, W.J. Brewerton, H. Brinkschulte, T. Brown, M. Brusati, T. Budd, M. Bures, P. Burton, T. Businaro, P. Butcher, H. Buttgereit, C. Caldwell-Nichols, D.J. Campbell, D. Campling, P. Card, G. Celentano, C.D. Challis, A.V.Chankin[23], A. Cherubini, D. Chiron, J. Christiansen, P. Chuilon, R. Claesen, S. Clement, E. Clipsham, J.P. Coad, I.H. Coffey[24], A. Colton, M. Comiskey[4], S. Conroy, M. Cooke, S. Cooper, J.G. Cordey, W. Core, G. Corrigan, S. Corti, A.E. Costley, G. Cottrell, M. Cox[7], P. Crawley, O. Da Costa, N. Davies, S.J. Davies[7], H. de Blank, H. de Esch, L. de Kock, E. Deksnis, N. Deliyanakus, G.B. Denne-Hinnov, G. Deschamps, W.J. Dickson[19], K.J. Dietz, A. Dines, S.L. Dmitrenko, M. Dmitrieva[25], J. Dobbing, N. Dolgetta, S.E. Dorling, P.G. Doyle, D.F. Düchs, H. Duquenoy, A. Edwards, J. Ehrenberg, A. Ekedahl, T. Elevant[11], S.K. Erents[7], L.G. Eriksson, H. Fajemirokun[12], H. Falter, J. Freiling[15], C. Froger, P. Froissard, K. Fullard, M. Gadeberg, A. Galetsas, L. Galbiati, D. Gambier, M. Garribba, P. Gaze, R. Giannella, A. Gibson, R.D. Gill, A. Girard, A. Gondhalekar, D. Goodall[7], C. Gormezano, N.A. Gottardi, C. Gowers, B.J. Green, R. Haange, A. Haigh, C.J. Hancock, P.J. Harbour, N.C. Hawkes[7], N.P. Hawkes[1], P. Haynes[7], J.L. Hemmerich, T. Hender[7], J. Hoekzema, L. Horton, J. How, P.J. Howarth[5], M. Huart, T.P. Hughes[4], M. Huguet, F. Hurd, K. Ida[18], B. Ingram, M. Irving, J. Jacquinot, H. Jaeckel, J.F. Jaeger, G. Janeschitz, Z. Jankowicz[22], O.N. Jarvis, F. Jensen, E.M. Jones, L.P.D.F. Jones, T.T.C. Jones, J-F. Junger, F. Junique, A. Kaye, B.E. Keen, M. Keilhacker, W. Kerner, N.J. Kidd, R. Konig, A. Konstantellos, P. Kupschus, R. Lässer, J.R. Last, B. Laundy, L. Lauro-Taroni, K. Lawson[7], M. Lennholm, J.Lingertat[13], R.N. Litunovski, A. Loarte, R. Lobel, P. Lomas, M. Loughlin, C. Lowry, A.C. Maas[15], B. Macklin, C.F. Maggi[16], G. Magyar, V. Marchese, F. Marcus, J. Mart, D. Martin, E. Martin, R. Martin-Solis[8], P. Massmann, G. Matthews, H. McBryan, G. McCracken[7], P. Meriguet, P. Miele, S.F. Mills, P. Millward, E. Minardi[16], R. Mohanti[17], P.L. Mondino, A. Montvai[3], P. Morgan, H. Morsi, G. Murphy, F. Nave[27], S. Neudatchin[23], G. Newbert, M. Newman, P. Nielsen, P. Noll, W. Obert, D. O'Brien, J. O'Rourke, R. Ostrom, M. Ottaviani, S. Papastergiou, D. Pasini, B. Patel, A. Peacock, N. Peacock[7], R.J.M. Pearce, D. Pearson[12], J.F. Peng[26], R. Pepe de Silva, G. Perinic, C. Perry, M.A. Pick, J. Plancoulaine, J-P. Poffé, R. Pohlchen, F. Porcelli, L. Porte[19], R. Prentice, S. Puppin, S. Putvinskii[23], G. Radford[9], T. Raimondi, M.C. Ramos de Andrade, M. Rapisarda[29], P-H. Rebut, R. Reichle, S. Richards, E. Righi, F. Rimini, A. Rolfe, R.T. Ross, L. Rossi, R. Russ, H.C. Sack, G. Sadler, G. Saibene, J.L. Salanave, G. Sanazzaro, A. Santagiustina, R. Sartori, C. Sborchia, P. Schild, M. Schmid, G. Schmidt[6], H. Schroepf, B. Schunke, S.M. Scott, A. Sibley, R. Simonini, A.C.C. Sips, P. Smeulders, R. Smith, M. Stamp, P. Stangeby[20], D.F. Start, C.A. Steed, D. Stork, P.E. Stott, P. Stubberfield, D. Summers, H. Summers[19], L. Svensson, J.A. Tagle[21], A. Tanga, A. Taroni, C. Terella, A. Tesini, P.R. Thomas, E. Thompson, K. Thomsen, P. Trevalion, B. Tubbing, F. Tibone, H. van der Beken, G. Vlases, M. von Hellermann, T. Wade, C. Walker, D. Ward, M.L. Watkins, M.J. Watson, S. Weber[10], J. Wesson, T.J. Wijnands, J. Wilks, D. Wilson, T. Winkel, R. Wolf, D. Wong, C. Woodward, M. Wykes, I.D. Young, L. Zannelli, A. Zolfaghari[28], G. Zullo, W. Zwingmann.

PERMANENT ADDRESSES

1. UKAEA, Harwell, Didcot, Oxon, UK.
2. University of Leicester, Leicester, UK.
3. Central Research Institute for Physics, Budapest, Hungary.
4. University of Essex, Colchester, UK.
5. University of Birmingham, Birmingham, UK.
6. Princeton Plasma Physics Laboratory, New Jersey, USA.
7. UKAEA Culham Laboratory, Abingdon, Oxon, UK.
8. Universidad Complutense de Madrid, Spain.
9. Institute of Mathematics, University of Oxford, UK.
10. Freien Universität, Berlin, F.R.G.
11. Royal Institute of Technology, Stockholm, Sweden.
12. Imperial College, University of London, UK.
13. Max Planck Institut für Plasmaphysik, Garching, FRG.
14. Risø National Laboratory, Denmark.
15. FOM Instituut voor Plasmafysica, Nieuwegein, The Netherlands.
16. Dipartimento di Fisica, University of Milan, Milano, Italy.
17. North Carolina State University, Raleigh, NC, USA
18. National Institute for Fusion Science, Nagoya, Japan.
19. University of Strathclyde, 107 Rottenrow, Glasgow, UK.
20. Institute for Aerospace Studies, University of Toronto, Ontario, Canada.
21. CIEMAT, Madrid, Spain.
22. Institute for Nuclear Studies, Otwock-Swierk, Poland.
23. Kurchatov Institute of Atomic Energy, Moscow, USSR
24. Queens University, Belfast, UK.
25. Keldysh Institute of Applied Mathematics, Moscow, USSR.
26. Institute of Plasma Physics, Academica Sinica, Hefei, P. R. China.
27. LNETI, Savacem, Portugal.
28. Plasma Fusion Center, M.I.T., Boston, USA.
29. ENEA, Frascati, Italy.

At 1st July, 1992